



Heriot-Watt University  
Research Gateway

## Multifunctional light sword metasurface lens

### Citation for published version:

Zhang, Z, Wen, D, Zhang, C, Chen, M, Wang, W, Chen, S & Chen, X 2018, 'Multifunctional light sword metasurface lens', *ACS Photonics*, vol. 5, no. 5, pp. 1794-1799.  
<https://doi.org/10.1021/acsp Photonics.7b01536>

### Digital Object Identifier (DOI):

[10.1021/acsp Photonics.7b01536](https://doi.org/10.1021/acsp Photonics.7b01536)

### Link:

[Link to publication record in Heriot-Watt Research Portal](#)

### Document Version:

Peer reviewed version

### Published In:

ACS Photonics

### Publisher Rights Statement:

This document is the Accepted Manuscript version of a Published Work that appeared in final form in ACS Photonics, copyright © American Chemical Society after peer review and technical editing by the publisher. To access the final edited and published work see <https://pubs.acs.org/doi/10.1021/acsp Photonics.7b01536>

### General rights

Copyright for the publications made accessible via Heriot-Watt Research Portal is retained by the author(s) and / or other copyright owners and it is a condition of accessing these publications that users recognise and abide by the legal requirements associated with these rights.

### Take down policy

Heriot-Watt University has made every reasonable effort to ensure that the content in Heriot-Watt Research Portal complies with UK legislation. If you believe that the public display of this file breaches copyright please contact [open.access@hw.ac.uk](mailto:open.access@hw.ac.uk) providing details, and we will remove access to the work immediately and investigate your claim.

## Multifunctional light sword metasurface lens

Zhengren Zhang, Dandan Wen, Chunmei Zhang, Ming Chen, Wei Wang, Shuqi Chen, and Xianzhong Chen

ACS Photonics, **Just Accepted Manuscript** • DOI: 10.1021/acsp Photonics.7b01536 • Publication Date (Web): 17 Mar 2018

Downloaded from <http://pubs.acs.org> on March 19, 2018

### Just Accepted

“Just Accepted” manuscripts have been peer-reviewed and accepted for publication. They are posted online prior to technical editing, formatting for publication and author proofing. The American Chemical Society provides “Just Accepted” as a service to the research community to expedite the dissemination of scientific material as soon as possible after acceptance. “Just Accepted” manuscripts appear in full in PDF format accompanied by an HTML abstract. “Just Accepted” manuscripts have been fully peer reviewed, but should not be considered the official version of record. They are citable by the Digital Object Identifier (DOI®). “Just Accepted” is an optional service offered to authors. Therefore, the “Just Accepted” Web site may not include all articles that will be published in the journal. After a manuscript is technically edited and formatted, it will be removed from the “Just Accepted” Web site and published as an ASAP article. Note that technical editing may introduce minor changes to the manuscript text and/or graphics which could affect content, and all legal disclaimers and ethical guidelines that apply to the journal pertain. ACS cannot be held responsible for errors or consequences arising from the use of information contained in these “Just Accepted” manuscripts.

## Multifunctional light sword metasurface lens

Zhengren Zhang<sup>1,2,†</sup>, Dandan Wen<sup>1,†</sup>, Chunmei Zhang<sup>1</sup>, Ming Chen<sup>3</sup>, Wei Wang<sup>1</sup>,

Shuqi Chen<sup>4</sup>, Xianzhong Chen<sup>1\*</sup>

1. SUPA, Institute of Photonics and Quantum Sciences, School of Engineering and Physical Sciences, Heriot-Watt University, Edinburgh, EH14 4AS, UK

2. School of Materials Science and Engineering, Chongqing Jiaotong University, Chongqing 400074, China

3. Centre for Photonics Research, Guilin University of Electronic Technology, Guilin, 541004, China

4. Laboratory of Weak Light Nonlinear Photonics Ministry of Education, School of Physics and Teda Applied Physics Institute, Nankai University, Tianjin 300071, China

### Abstract

The depth of focus of an imaging system determines the range of change for both the position of focal plane and image plane. Although a typical light sword optical element with angular modulation of phase transmittance can extend its focus of depth due to its angular variation of the optical power, it lacks rotational symmetry and exhibits a junction, rendering its fabrication extremely difficult. Optical metasurfaces provide an unusual approach to develop such a device due to their unprecedented capability in the manipulation of light propagation in a desirable manner. We propose and experimentally demonstrate a light sword metasurface lens with multiple functionalities. The position of focal segments can be controlled by changing the polarization state of the incident light. The developed ultrathin, ultraflat device can facilitate device miniaturization and system integration and may find applications in various fields such as optical coupling, imaging, and interconnections.

**Key words:** Metasurface, light sword lens, multiple functionalities, long focus of depth.

<sup>†</sup> These authors contribute equally to this work.

\* Email: [x.chen@hw.ac.uk](mailto:x.chen@hw.ac.uk)

1  
2  
3 Depth of focus is one of important parameters for an imaging system, which  
4 determines the range of change for the position of focal plane and image plane.  
5  
6 Extending depth of focus of lens has attracted much attention due to its practical  
7 applications. Various methods have been proposed to produce an optical element with  
8 long depth of focus, including Yang-Gu algorithm<sup>1</sup>, inverse quartic axicon<sup>2</sup> and light  
9 sword optical element (LSOE)<sup>3,4</sup>. In contrast to other solutions, LSOEs have  
10 demonstrated their superiority especially for multifocal imaging with extended depth  
11 of focus<sup>5</sup>. LSOEs are distinguished by angular variation of the optical power since  
12 every infinitesimal angular sector has its own focal length, leading to the  
13 independence of their optical power range with respect to the pupil's diameter. These  
14 devices are typically made by fabricating a transparent substrate at different depths to  
15 yield a desired phase profile in the transmitted light. However, LSOEs lack rotational  
16 symmetry and exhibit a junction, rendering their fabrication extremely difficult. For  
17 example, the surface curvature of such an element continuously and smoothly varies  
18 across the entire surface, which results in the discontinuity observed as a radially  
19 placed edge. There are technical challenges for manufacturing to accurately produce  
20 such a smooth, continuous surface with a sharp edge. Furthermore, the sharp edge  
21 may hinder its applications in system integration since it must be handled with  
22 extreme care, which increases the difficulty level for system assembly. Although  
23 diffractive optical elements have the advantage of being relatively flat, their  
24 fabrication process is not suitable for the light sword devices since they are highly  
25 susceptible to fabrication errors, especially at a point where a big phase change jump  
26 is required.  
27  
28  
29  
30  
31  
32  
33  
34  
35  
36  
37  
38  
39  
40  
41  
42  
43  
44  
45  
46

47 Optical metasurfaces, which are two-dimensional counterparts of metamaterials with  
48 subwavelength thickness, have aroused considerable interest since they can control  
49 light propagation in a desirable manner, providing a viable route to develop ultrathin,  
50 ultraflat optical devices<sup>6-15</sup>. Metasurfaces consist of a single layer or few-layer stacks  
51 of artificial planar structures and can engineer the amplitude, phase and polarization  
52 of a light beam at subwavelength resolution, making them possible to solve the  
53  
54  
55  
56  
57  
58  
59  
60

1  
2  
3 fabrication challenge in optical devices based on phase accumulation due to the  
4 propagation effect<sup>16-18</sup>. A plethora of applications on metasurfaces have been  
5 proposed and demonstrated, such as beam shaper<sup>19</sup>, orbital angular momentum  
6 manipulation<sup>20, 21</sup>, ultrathin metalenses<sup>17, 22</sup>, spin Hall effect of light<sup>23</sup>, and optical  
7 holography<sup>8, 11, 13, 24</sup>. To tackle the technical fabrication challenge in LSOEs, we  
8 propose and experimentally demonstrate a facile metasurface approach to develop  
9 multifunctional light sword metasurface lens (MLSMLs). In comparison with  
10 traditional bulky LSOEs with wavelength-dependent phase profile based on optical  
11 path difference, the developed MLSMLs are ultrathin, ultraflat and ideal for device  
12 miniaturization and system integration. Although using optical metasurfaces to design  
13 polarization-controlled lens with needle-shaped focal points has been theoretically  
14 proposed<sup>25</sup>, it hasn't been experimentally demonstrated. Furthermore, unlike  
15 previously demonstrated LSOEs, the functionality of the fabricated device here can be  
16 changed by controlling the polarization state of the incident light. Our demonstrated  
17 results might enable new types of ultracompact optical elements for generating  
18 LSOEs with long focus of depth, and also advance metasurface based multifunctional  
19 devices.  
20  
21  
22  
23  
24  
25  
26  
27  
28  
29  
30  
31  
32  
33  
34  
35

## 36 **Design and Methods**

37  
38  
39

40 Figure 1 shows the schematic of the MLSML when illuminated by a linearly polarized  
41 light beam at normal incidence. The unique metasurface device here functions as a  
42 combination of two separate LSOEs since it has two different focal lengths with same  
43 focal range ( $\Delta f$ ) for circularly polarized light with opposite helicity (left-handed and  
44 right-handed circular polarizations, LCP and RCP). Each infinitesimal angular sector  
45 on the individual device is equivalent to a Fresnel lens with a focal length  $f + \Delta f\theta/2\pi$ ,  
46 where  $\theta$  is the azimuthal angle. A circularly polarized light beam can be focused into  
47 one of focal segments stretched from  $f$  up to  $f+\Delta f$  by such an optical element. The two  
48 separate focal segments correspond to the incident light with different circular  
49 polarizations. Upon the illumination of a linearly polarized light beam, two focal  
50  
51  
52  
53  
54  
55  
56  
57  
58  
59  
60

segments are obtained since it can be decomposed into LCP light and RCP light with same components. Thus, the focal segments of the designed device can be changed by controlling the polarization state of the incident light. To achieve the desired phase profile while maintaining uniform amplitude, a metasurface consisting of gold nanorods with spatially variant orientations is used. When an incident circularly polarized beam normally passes through the anisotropic nanorods, the transmitted beam contains both the original spin part without phase shift and the converted spin part with the induced phase shift (known as Pancharatnam-Berry phase). The additional phase delay is  $\pm 2\varphi$  ( $\varphi$  is the orientation angle of nanorod) for the cross-polarization (RCP/LCP) transmitted waves, where the plus/minus sign is decided by the helicity of the incident light<sup>17</sup>.

The phase transmittance of the MLSML is defined by the following relation<sup>26, 27</sup>:

$$\varphi(r, \theta) = \pm \frac{kr^2}{2[f + (\Delta f \theta / 2\pi)]} \quad (1)$$

where  $r, \theta$  are the radial and azimuthal coordinate, respectively. The angle  $\theta$  ranges from 0 to  $2\pi$ .  $k = 2\pi/\lambda$  is the free-space wave vector, and  $\lambda$  is the wavelength of the incident light. The parameters  $f$  and  $\Delta f$  represent the focal length and the focal range of the element, respectively. From the equation (1), we can see that each infinitesimal angular sector is equivalent to a Fresnel lens with a focal length  $f + \Delta f \theta / 2\pi$ . Therefore the LSOE-based metasurface lens can focus approximately a plane wave into a focal segment stretched from  $f$  up to  $f + \Delta f$ . Note that the '+' and '-' signs in Eq. (1) correspond to a positive (convex) and negative (concave) polarity, respectively, for the incident LCP and RCP light. To design such a multifunctional device, two metasurfaces (each one for a specific focal segment) are designed to operate with opposite incident helicities and merged together with a displacement. Suppose  $d_1$  is the distance between neighboring nanorods with a value of 424 nm along both  $x$  and  $y$  directions, the displacement vector is  $(d_1/2, d_1/2)$ , as detailed in Fig. 2. Each gold nanorod is 200 nm long, 70 nm wide, and 40 nm thick. There are two

1  
2  
3 separate metasurfaces that can generate two different types of required phase profiles,  
4 but the size of the sample before and after metasurface merging is the same and the  
5 equivalent pixel size in the merged metasurface is  $300\text{ nm}\times 300\text{ nm}$ . Indium-tin-oxide  
6 (ITO) coated glass substrates are used to fabricate the designed nanorod structures.  
7 Nanostructures are defined in a positive PMMA resist film on glass substrates using  
8 standard electron-beam lithography. Then a 40 nm gold film is deposited on the  
9 sample via electron beam evaporation. Finally, the metasurface consisting of gold  
10 nanorods is achieved by a subsequent lift-off procedure. Fig. 2(f) shows the scanning  
11 electron microscopy (SEM) image of part of our fabricated multifunctional device.  
12 Fig. 2(c), (d) and (g) are the magnified figures for the regions A, B and C, respectively.  
13 Fig. 2(c) and (d) clearly shows the phase-edge of our light sword metasurface lens  
14 (similar to traditional light sword lenses).  
15  
16  
17  
18  
19  
20  
21  
22  
23  
24  
25  
26

### 27 **Results and Discussions**

28 Under the illumination of LCP light and RCP light at normal incidence, the simulation  
29 and experimental results for light focusing with long focus of depth at the wavelength  
30 of 650 nm are shown in Fig. 3. The converted part with phase change is characterized  
31 by filtering out the non-converted part in our experiment. The focal lengths for LCP  
32 and RCP light are chosen to be  $1400\text{ }\mu\text{m}$  and  $1500\text{ }\mu\text{m}$ , respectively. However, their  
33 focal range  $\Delta f$  is the same ( $50\text{ }\mu\text{m}$ ). To generate two LSOEs with different polarity  
34 for the same circular polarization (e.g., LCP), the signs of the phase profile for the  
35 two optical elements are chosen to be “+” and “-”, respectively (as shown in Eq.(1)).  
36 Therefore, only one real focal segment is expected when an incident light beam with  
37 pure circular polarization (LCP or RCP) shines on the sample. To further analyze the  
38 characteristic of long focus depth, the light intensity distributions along the  
39 longitudinal direction at the positions of  $1375\text{ }\mu\text{m}$ ,  $1400\text{ }\mu\text{m}$ , and  $1425\text{ }\mu\text{m}$  (marked by  
40 regions I, II, III) are also given in Fig. 3a. The three focal spots in the transverse plane  
41 unambiguously show that the designed device has a long focus of depth. Similarly,  
42 another real focal segment is predicted if the polarization state of the incident light is  
43  
44  
45  
46  
47  
48  
49  
50  
51  
52  
53  
54  
55  
56  
57  
58  
59  
60

1  
2  
3 changed from LCP to RCP. The light intensity distributions along the longitudinal  
4 direction at the positions of at the location of 1475  $\mu\text{m}$ , 1500  $\mu\text{m}$ , and 1525  $\mu\text{m}$   
5 (marked by IV, V, VI) are also given (see Fig. 3(b)). The experimental setup to  
6 characterize the fabricated metasurface device is shown in Figure S1 (Supplementary  
7 Section). The sample is mounted on a 3D translation stage, allowing for fine  
8 adjustment. The incident light at the wavelength of 650 nm is from a tunable  
9 supercontinuum laser source (NKT-SuperK EXTREME). The required polarization  
10 state is generated by a polarizer and a quarter-wave plate. Since the sign of the phase  
11 profile can be flipped by controlling the helicity of the incident light, the focal  
12 segments will be swapped along the longitudinal direction when the helicity of the  
13 incident light is changed from LCP to RCP (shown in Fig. 3b). The full width at half  
14 maximum (FWHM) is an important parameter commonly used to describe the spot  
15 size of a focal point. The simulated FWHMs for the three real focal points in regions I,  
16 II, and III in Fig.3(a) are 3.6  $\mu\text{m}$ , 4.2  $\mu\text{m}$ , and 4.2  $\mu\text{m}$ , respectively. In contrast, the  
17 experimental measured FWHMs are 5.7  $\mu\text{m}$ , 6.03  $\mu\text{m}$ , and 6.03  $\mu\text{m}$ , respectively. The  
18 measured FWHMs for IV, V and VI are that 5.03  $\mu\text{m}$ , 4.2  $\mu\text{m}$ , and 6.7  $\mu\text{m}$ ,  
19 respectively, while the corresponding simulated values are 4  $\mu\text{m}$ , 4.2  $\mu\text{m}$ , and 4.4  $\mu\text{m}$ ,  
20 respectively. The deviation is mainly due to the fabrication error and measurement  
21 accuracy. Nevertheless, good agreement between simulation and experiment is found.  
22  
23  
24  
25  
26  
27  
28  
29  
30  
31  
32  
33  
34  
35  
36  
37  
38  
39

40 We further characterize the performance of the developed device for the incident light  
41 with linear polarization. Figure 4(b) shows the experimentally measured intensity  
42 distributions at six longitudinal positions marked by I-VI, corresponding to 1375  $\mu\text{m}$ ,  
43 1400  $\mu\text{m}$ , 1425  $\mu\text{m}$ , 1475  $\mu\text{m}$ , 1500  $\mu\text{m}$ , and 1525  $\mu\text{m}$ , respectively. The regions I-III  
44 belong to the first focal segment and the regions IV-VI belong to the second one, as  
45 shown in Fig. 4(a). Their light intensity distributions have similar tendency as shown  
46 in Fig. 3(a) and (b) except for the regions III and IV. The light intensities in region III  
47 and IV shown in Fig. 4(b) are stronger than those in Fig.3(a) and (b), which is due to  
48 the fact that the distance between the two focal segments is relatively close and results  
49 in intensity overlap in these regions.  
50  
51  
52  
53  
54  
55  
56  
57  
58  
59  
60



1  
2  
3  
4  
5 The conversion efficiency between the two circular polarization states is an important  
6 parameter in the performance of the metasurface device. This value is defined as the  
7 ratio of the power of the helicity-changed light (e.g., from LCP to RCP or RCP to  
8 LCP) to that of the input light. It is worth mentioning that the efficiency of the device  
9 is halved since a linearly polarized light beam can be decomposed into two circularly  
10 polarized lights beams with opposite helicity. As a proof-of-concept, the conversion  
11 efficiency between the polarization states based on the plasmonic metasurface is  
12 measured to be 2% at 650 nm, which is at the lower edge of what is required for  
13 practical applications. As an alternative to metallic nanorods, however, a dielectric  
14 metasurface can be used to dramatically increase this value since it can decrease the  
15 ohmic losses and improve the scattering cross sections of the metal nanorods<sup>28,29</sup>.

16 An interesting question is whether there is a limit in the depth of focus in this design.  
17 Each infinitesimal angular sector on the metasurface device is equivalent to a Fresnel  
18 lens with a specific focal length. With the increase of the depth of focus, the phase  
19 difference between unit cells will be insufficient, leading to the decrease of energy in  
20 each focal plane along the longitudinal direction within the depth of focus.  
21 Furthermore, the background noise will increase and the contrast will become worse.  
22 Our design is based on transmission mode, while Veysi's work is based on reflective  
23 operation<sup>25</sup>, which is not compatible with most optical systems that operate in the  
24 transmission mode. In addition, the multiple functionality in our work is realized by  
25 controlling circular polarization of the incident light, instead of linear polarization in  
26 Veysi's work. Furthermore, in comparison with Y-shaped structures proposed by Veysi,  
27 nanorod structures are much simpler, which can facilitate nanofabrication.

## 28 29 30 31 32 33 34 35 36 37 38 39 40 41 42 43 44 45 46 47 48 49 **Conclusion**

50 In conclusion, we have theoretically and experimentally demonstrated a facile  
51 metasurface approach to realize a light sword lens with multiple functionalities based  
52 on the geometric design and arrangement of light-scattering nano-antennas. The  
53 desired phase profile is realized by a metasurface consisting of nanorods with  
54  
55  
56  
57  
58  
59  
60

1  
2  
3 spatially variant orientation. The functionality of the fabricated ultrathin, flat light  
4 sword metasurface device can be controlled by changing the polarization state of the  
5 incident light, which enables the realization of novel optical components with  
6 functionalities tailored to specific applications. The fabrication procedure is  
7 compatible with standard semiconductor fabrication process and the compact device  
8 can facilitate device miniaturization and system integration, which may find  
9 applications in optical coupling, imaging, and interconnections.  
10  
11  
12  
13  
14  
15  
16  
17

### 18 **Acknowledgments**

19  
20  
21 X.C. acknowledges the Engineering and Physical Sciences Research Council of the  
22 United Kingdom (Grant Ref: EP/ P029892/1). Z.Z. would like to acknowledge  
23 National Natural Science Foundation of China (Grant No. 11504034), Chongqing  
24 Research Program of Basic Research and Frontier Technology (Grant No.  
25 cstc2016jcyjA0186) and financial support from the China Scholarship Council (Grant  
26 No. 201608500036).  
27  
28  
29  
30  
31  
32  
33  
34  
35  
36  
37

### 38 **References**

- 39  
40 [1] Dong, B. Z.; Yang, G. Z.; Gu, B. Y.; Ersoy, O. K. Iterative optimization approach  
41 for designing an axicon with long focal depth and high transverse resolution. *J. Opt.*  
42 *Soc. Am. A* **1996**, *13*, 97-103.  
43  
44 [2] Ares, J.; Flores, R.; Bará, S.; Jaroszewicz, Z. Presbyopia compensation with a  
45 quartic axicon. *Optom. Vis. Sci.* **2005**, *82*, 1071-1078.  
46  
47 [3] Petelczyc, K.; Bará, S.; Lopez, A. C.; Jaroszewicz, Z.; Kakarenko, K.;  
48 Kołodziejczyk, A.; Sypek, M. Imaging properties of the light sword optical element  
49 used as a contact lens in a presbyopic eye model. *Opt. Express* **2011**, *19*,  
50 25602-25616.  
51  
52 [4] Kołodziejczyk, A.; Bará, S.; Jaroszewicz, Z.; and Sypek, M. The light sword  
53  
54  
55  
56  
57  
58  
59  
60

1  
2  
3 optical element—a new diffraction structure with extended depth of focus. *J.*  
4 *Mod. Opt.* **1990**, *37*, 1283-1286.

5  
6 [5] Kakarenko, K.; Ducin, I.; Grabowiecki, K.; Jaroszewicz, Z.; Kolodziejczyk, A.;  
7 Mira-Agudelo, A.; Petelczyc, K.; Składowska, A; Sypek, M. Assessment of imaging  
8 with extended depth-of-field by means of the light sword lens in terms of visual acuity  
9 scale. *Biomed. Opt. Express* **2015**, *6*, 1738-1748.

10  
11 [6] Yu, N.; Genevet, P.; Kats, M. A.; Aieta, F.; Tetienne, J. P.; Capasso, F.; Gaburro,  
12 Z. Light propagation with phase discontinuities: generalized laws of reflection and  
13 refraction. *Science* **2011**, *334*, 333-337.

14  
15 [7] Huang, L.; Chen, X.; Mühlenbernd, H.; Li, G.; Bai, B.; Tan, Q.; Jin, G.; Zentgraf,  
16 T.; Zhang, S. Dispersionless phase discontinuities for controlling light propagation.  
17 *Nano Lett.* **2012**, *12*, 5750-5755.

18  
19 [8] Zheng, G.; Mühlenbernd, H.; Kenney, M.; Li, G.; Zentgraf, T.; Zhang, S.  
20 Metasurface holograms reaching 80% efficiency. *Nat. Nanotechnol.* **2015**, *10*,  
21 308-312.

22  
23 [9] Ni, X.; Wong, Z. J.; Mrejen, M.; Wang, Y.; Zhang, X. An ultrathin invisibility  
24 skin cloak for visible light. *Science* **2015**, *349*, 1310-1314.

25  
26 [10] Genevet, P.; Capasso F, Aieta, F.; Khorasaninejad, M.; Devlin, R. Recent  
27 advances in planar optics: from plasmonic to dielectric metasurfaces. *Optica* **2017**, *4*,  
28 139-152.

29  
30 [11] Chen, W. T.; Yang, K. Y.; Wang, C. M.; Huang, Y. W.; Sun, G.; Chiang, I. D.;  
31 Liao, C. Y.; Hsu, W. L.; Lin, H. T.; Sun, S.; Zhou, L. High-efficiency broadband  
32 meta-hologram with polarization-controlled dual images. *Nano Lett.* **2013**, *14*,  
33 225-230.

34  
35 [12] Sun, S.; He, Q.; Xiao, S.; Xu, Q.; Li, X.; Zhou, L. Gradient-index meta-surfaces  
36 as a bridge linking propagating waves and surface waves. *Nat. Mater.* **2012**, *11*,  
37 426-431.

38  
39 [13] Hu, D.; Wang, X.; Feng, S.; Ye, J.; Sun, W.; Kan, Q.; Klar, P. J.; Zhang, Y.  
40 Ultrathin terahertz planar elements. *Adv. Opt. Mater.* **2013**, *1*, 186-191.

41  
42 [14] Li, J.; Chen, S.; Yang, H.; Li, J.; Yu, P.; Cheng, H.; Gu, C.; Chen, H. T.; Tian, J.

1  
2  
3 Simultaneous control of light polarization and phase distributions using plasmonic  
4 metasurfaces. *Adv. Funct. Mater.* **2015**, *25*, 704-710.

5  
6 [15] Liu, L.; Zhang, X.; Kenney, M.; Su, X.; Xu, N.; Ouyang, C.; Shi, Y.; Han, J.;  
7 Zhang, W.; Zhang, S. Broadband metasurfaces with simultaneous control of phase  
8 and amplitude. *Adv. Mater.* **2014**, *26*, 5031-5036.

9  
10 [16] Li, G; Zhang, S; Zentgraf, T. Nonlinear photonic metasurfaces. *Nat. Rev. Mater.*  
11 **2017**, *2*, 17010.

12 [17] Chen, X.; Huang, L; Mühlenbernd, H.; Li, G.; Bai, B.; Tan, Q.; Jin, G; Qiu, C;  
13 Zhang, S; Zentgraf, T. Dual-polarity plasmonic metalens for visible light. *Nat.*  
14 *Commun.* **2012**, *3*, 1198.

15 [18] Wen, D.; Yue, F.; Li, G.; Zheng, G.; Chan, K.; Chen, S.; Chen, M; King Fai Li,  
16 K. F.; Wong, P. W. H.; Cheah, K. W.; Pun, E. Y. B.; Zhang, S; Chen, X. Helicity  
17 multiplexed broadband metasurface holograms. *Nat. Commun.* **2015**, *6*, 8241.

18 [19] Chen, X.; Zhang, Y.; Huang, L.; Zhang, S. Ultrathin metasurface laser beam  
19 shaper. *Adv. Opt. Mater.* **2014**, *2*, 978-982.

20 [20] Yue, F.; Wen, D.; Zhang, C.; Gerardot, B. D.; Wang, W.; Zhang, S.; Chen, X.;  
21 Multichannel Polarization-Controllable Superpositions of Orbital Angular Momentum  
22 States. *Adv. Mater.* **2017**, *29*, 1603838.

23 [21] Ma, X.; Pu, M., Li, X.; Huang, C.; Wang, Y.; Pan, W.; Zhao, B.; Cui, J.; Wang,  
24 C.; Zhao, Z.; and Luo, X. A planar chiral meta-surface for optical vortex generation  
25 and focusing. *Sci. Rep.* **2015**, *5*, 10365.

26 [22] Aieta, F.; Genevet, P.; Kats, M. A.; Yu, N.; Blanchard, R.; Gaburro, Z.; Capasso,  
27 F. Aberration-free ultrathin flat lenses and axicons at telecom wavelengths based on  
28 plasmonic metasurfaces. *Nano Lett.* **2012**, *12*, 4932-4936.

29 [23] Yin, X.; Ye, Z.; Rho, J.; Wang, Y.; Zhang, X. Photonic spin Hall effect at  
30 metasurfaces. *Science* **2013**, *339*, 1405-1407.

31 [24] Larouche, S.; Tsai, Y. J.; Tyler, T.; Jokerst, N. M.; Smith, D. R. Infrared  
32 metamaterial phase holograms. *Nat. Mater.* **2012**, *11*, 450-454.

33 [25] Veysi, M.; Guclu, C.; Boyraz, O.; and Capolino, F. Reflective metasurface lens  
34 with an elongated needle-shaped focus. *J. Opt. Soc. Am. B*, **2017**, *34*, 374-382.

- 1  
2  
3 [26] Petelczyc, K.; Garcia, J. A.; Bara, S.; Jaroszewicz, Z.; Kakarenko, K.;  
4 Kolodziejczyk, A.; Sypek, M. Strehl ratios characterizing optical elements designed  
5 for presbyopia compensation. *Opt. Express* **2011**, *19*, 8693-8699.  
6  
7  
8 [27] Petelczyc, K.; Garcia, J. A.; Bará, S.; Jaroszewicz, Z.; Kołodziejczyk, A.; Sypek,  
9 M. Presbyopia compensation with a light sword optical element of a variable diameter.  
10 *Photonics Letters of Poland* **2009**, *1*, 55-57.  
11  
12 [28] Khorasaninejad, M.; Chen, W.T.; Devlin, R.C.; Oh, J.; Zhu, A.Y. and Capasso, F.  
13 Metalenses at visible wavelengths: Diffraction-limited focusing and subwavelength  
14 resolution imaging. *Science* **2016**. 352, 1190-1194.  
15  
16 [29] Arbabi, A.; Horie, Y.; Bagheri, M.; Faraon, A. Dielectric metasurfaces for  
17 complete control of phase and polarization with subwavelength spatial resolution and  
18 high transmission. *Nat. Nanotechnol.*, **2015**, *10*, 937-943.  
19  
20  
21  
22  
23  
24  
25  
26  
27  
28  
29  
30  
31  
32  
33  
34  
35  
36  
37  
38  
39  
40  
41  
42  
43  
44  
45  
46  
47  
48  
49  
50  
51  
52  
53  
54  
55  
56  
57  
58  
59  
60

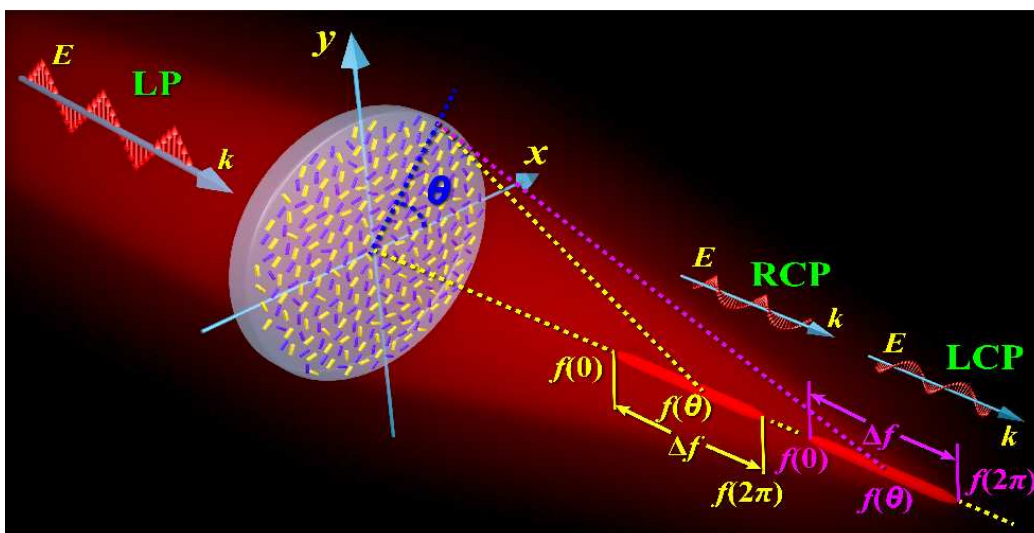


Fig. 1. Schematic of multifunctional light sword metasurface lens. Each infinitesimal angular sector is equivalent to a Fresnel lens with a focal length  $f + \Delta f \theta / 2\pi$ , where  $f$ ,  $\Delta f$  and  $\theta$  represent focal length, focal range and azimuthal coordinate, respectively. Upon the illumination of an incident light with linear polarization (LP), the device has two real focal segments corresponding to the transmitted light with right circular polarization (RCP) and left circular polarization (LCP). The metasurface consists of gold nanorods with spatially-varying orientation.

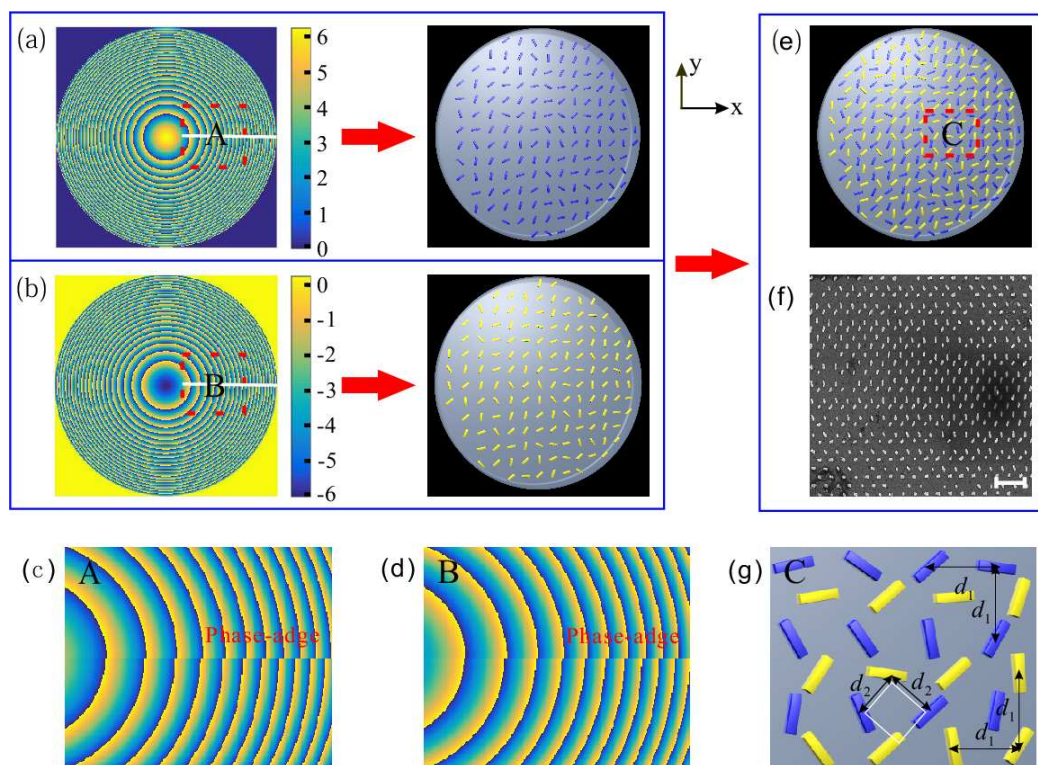


Fig.2. Generation of the multifunctional light sword metasurface lens and scanning electron microscopy (SEM) image of the sample. Suppose  $d_1$  is the distance between neighboring antennas with a value of 424 nm along x and y directions. Two sets of light sword metasurface lenses are designed to operate with opposite incident helicities and merged together with a displacement vector of  $(d_1/2, d_1/2)$ .  $d_2$  is the equivalent distance between neighbouring nanorods in the merged metasurface, which is 300 nm. Upon the illumination of LCP light at normal incidence, the signs of generated phase profiles for the transmitted lights beams are (a) positive and (b) negative, respectively. (e) Schematic of the merged metasurface. (f) SEM image of part of the multifunctional metasurface lens. The scale bar is 1  $\mu\text{m}$ . (c) and (d) show the phase distributions in the regions of A and B marked by the dotted rectangles, respectively. (g) The nanorod distribution in the region C.

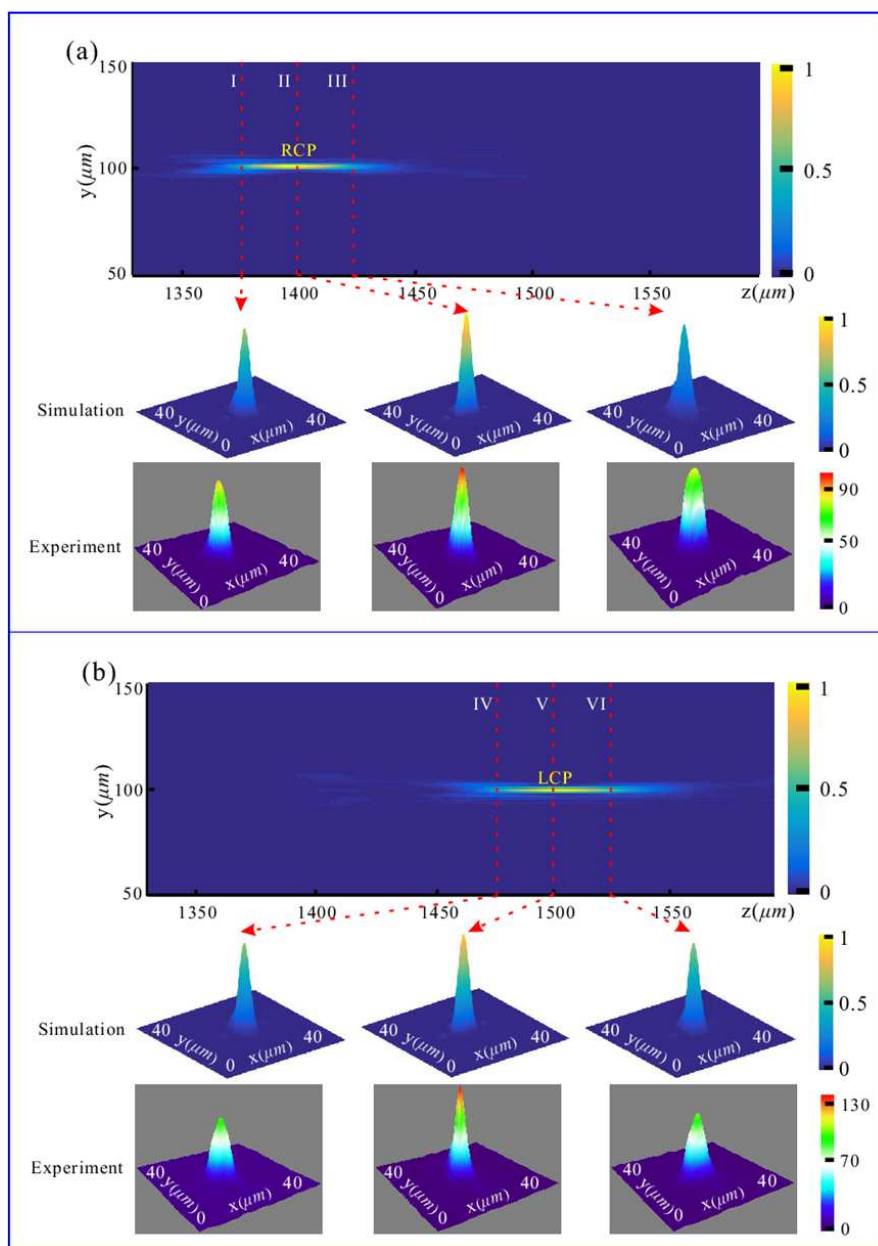


Fig.3. Simulation and experimental results of the multifunctional metasurface device at 650 nm. (a) The focusing performance of the metasurface lens when illuminated by an incident light with left circular polarization (LCP) at normal incidence. Theoretical and measured intensity distributions in the three focal planes located at longitudinal positions of 1375  $\mu\text{m}$ , 1400  $\mu\text{m}$ , and 1425  $\mu\text{m}$  (marked by region I, II, III) are also given. (b) Simulation and experimental results for the incident light with right circular polarization (RCP).



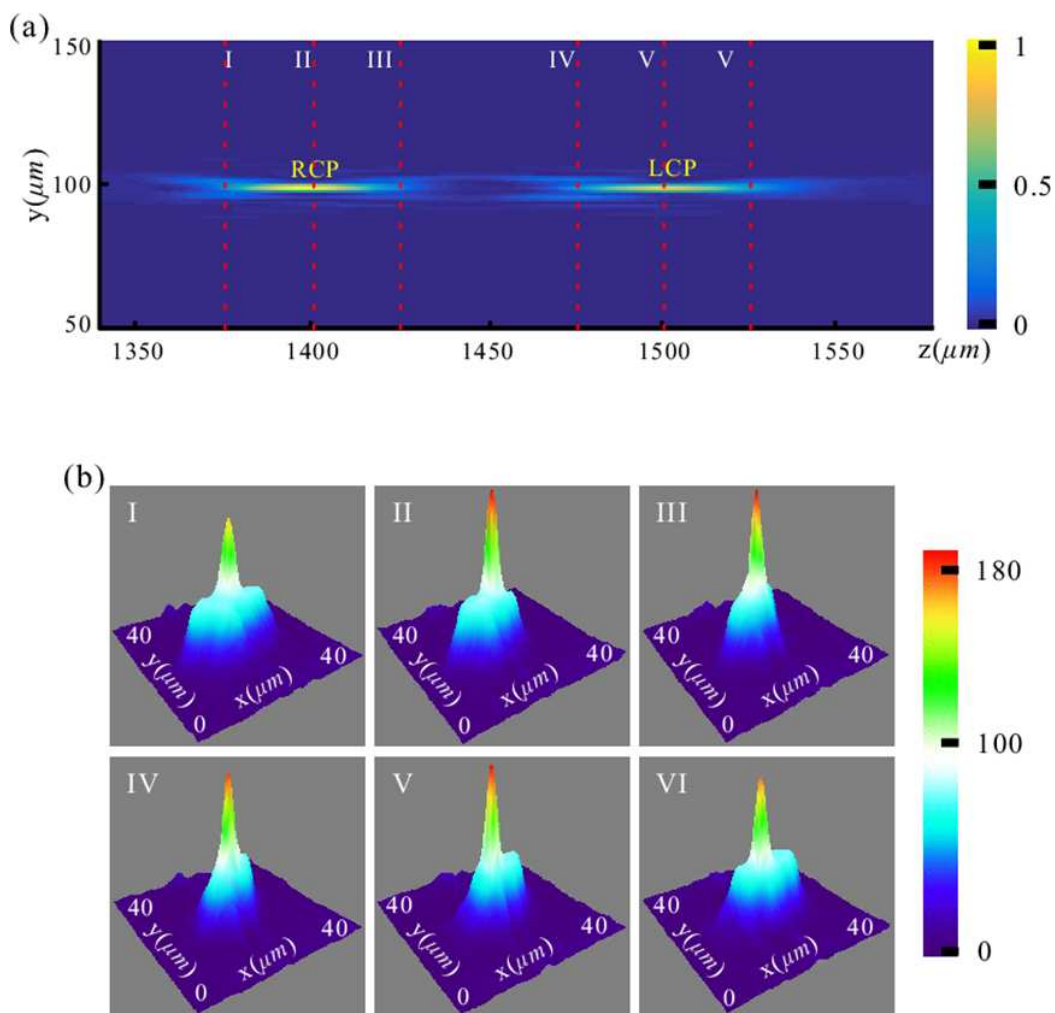
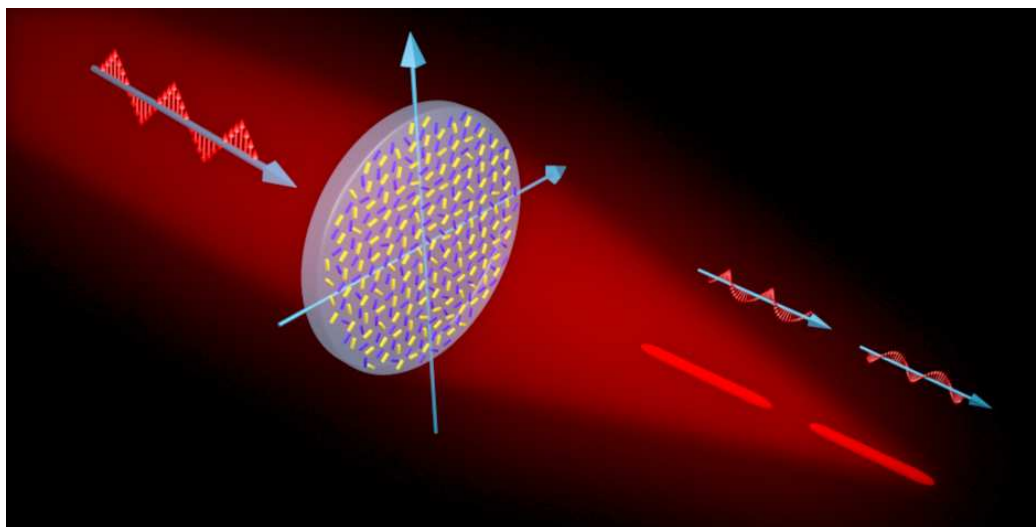


Fig.4. Simulation and experimentally measured results for the incident light with linear polarization. (a) Two focal segments for light with different helicities are observed in the simulation since a linearly polarized light can be decomposed into a LCP light beam and a RCP light beam with same components. (b) Experimentally measured intensity distributions in the focal planes located at 6 longitudinal positions.

**For Table of Contents Use Only****Multifunctional light sword metasurface lens**

Zhengren Zhang<sup>1,2,†</sup>, Dandan Wen<sup>1,†</sup>, Chunmei Zhang<sup>1</sup>, Ming Chen<sup>3</sup>, Wei Wang<sup>1</sup>,  
Shuqi Chen<sup>4</sup>, Xianzhong Chen<sup>1\*</sup>

1. SUPA, Institute of Photonics and Quantum Sciences, School of Engineering and Physical Sciences, Heriot-Watt University, Edinburgh, EH14 4AS, UK
2. School of Materials Science and Engineering, Chongqing Jiaotong University, Chongqing 400074, China
3. Centre for Photonics Research, Guilin University of Electronic Technology, Guilin, 541004, China
4. Laboratory of Weak Light Nonlinear Photonics Ministry of Education, School of Physics and Teda Applied Physics Institute, Nankai University, Tianjin 300071, China

**Description:**

This schematic shows the multifunctional light sword metasurface lens when illuminated by a linearly polarized light beam at normal incidence. The metasurface device here functions as a combination of two separate light sword lenses since it has two different focal lengths with same focal range for circularly polarized light with opposite helicity. Each infinitesimal angular sector on the individual device is equivalent to a Fresnel lens with a specific focal length. A circularly polarized light beam can be focused into one of focal segments by such an optical element. The two separate focal segments correspond to the incident light with different circular polarizations. Upon the illumination of a linearly polarized light beam, two focal segments are obtained. Thus, the focal segments of the designed device can be changed by controlling the polarization state of the incident light.